Article

Novel "Potentially Antiaromatic", Acidichromic Quinonediimines with Tunable Delocalization of Their 6π-Electron Subunits

Olivier Siri, Pierre Braunstein, Marie-Madeleine Rohmer, Marc Bnard, and Richard Welter

J. Am. Chem. Soc., **2003**, 125 (45), 13793-13803• DOI: 10.1021/ja035463u • Publication Date (Web): 16 October 2003

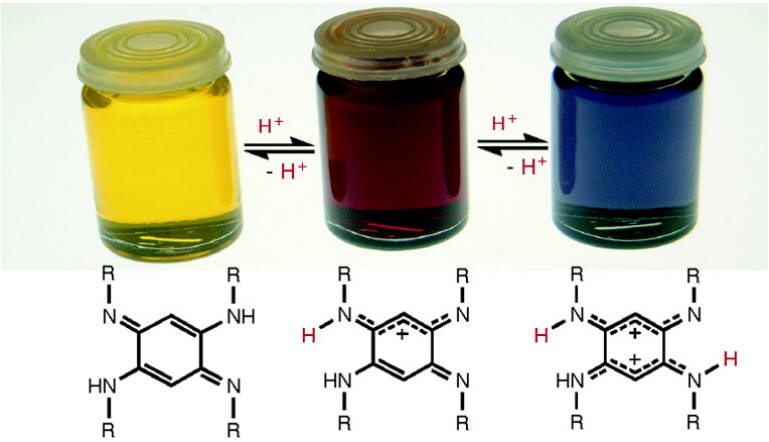

More About This Article

Additional resources and features associated with this article are available within the HTML version:

- Supporting Information
- Links to the 5 articles that cite this article, as of the time of this article download
- Access to high resolution figures
- Links to articles and content related to this article
- Copyright permission to reproduce figures and/or text from this article

View the Full Text HTML

J|A|C|S
ARTICLES
Published on Web 10/16/2003

Novel "Potentially Antiaromatic", Acidichromic Quinonediimines with Tunable Delocalization of Their 6π-Electron Subunits

Olivier Siri,[†] Pierre Braunstein,*[,†] Marie-Madeleine Rohmer,[‡] Marc Bénard,[‡] and Richard Welter[§]

Contribution from the Laboratoire de Chimie de Coordination, UMR 7513 CNRS, Université Louis Pasteur, 4, rue Blaise Pascal, 67070 Strasbourg Cedex, France, the Laboratoire de Chimie Quantique, UMR 7551 CNRS, Université Louis Pasteur, 4, rue Blaise Pascal, F-67070 Strasbourg Cedex, France, and the Laboratoire DECMET, UMR 7513 CNRS, Université Louis Pasteur, 4, rue Blaise Pascal, F-67070 Strasbourg Cedex, France

Received April 4, 2003; E-mail: braunst@chimie.u-strasbg.fr

Abstract: We present a novel family of "potentially antiaromatic" alkyl-substituted *p*-benzoquinonediimine pH-dependent chromophores. It appears from the structural data that these overall 12π-electron molecules should be better considered as constituted by two chemically connected but electronically not conjugated 6π-electron subunits. Molecule **5** appears to be the first example of two separated, conjugated, and localized 6π-electron systems that can be tuned by reversible protonation to become delocalized. The mono- and diprotonated derivatives have been characterized by spectroscopic methods and X-ray diffraction. These systems develop supramolecular interactions in the solid state that clearly reflect the degree of protonation and depend on the nature of the counterion. These compounds constitute new chromophores for which the color can be tuned depending on the degree of protonation, going in solution from yellow for **5** to red for **5**·HCl and blue for **5**·2HCl. Theoretical calculations have provided a deeper insight into the electronic structure of these molecules and allowed an assignment of the experimental UV−vis spectra. The visible and near-UV spectrum of the neutral and protonated benzoquinonediimines can be classically assigned from the coupling of two 6π-electron polymethine units. TD-DFT calculations confirm the observed red shift of the two lowest $\pi \rightarrow \pi^*$ transitions of the benzoquinonediimines upon protonation and relate it to the moderate energy lowering of the HOMO → LUMO transition induced by the delocalization of the polymethine π system.

Introduction

Research on the relation between color and structure in organic compounds has received a great deal of attention for decades.[1−3] In 1926, the polymethine structure was recognized by König as the true origin of color.[4] Designing molecules with controlled colors may result from fine-tuning of the photophysical characteristics of a given family of organic chromophores.[5] For example, conjugated oligomers and polymers permit color tuning through chemical or structural modifications.[6] A simple color test of enantiomeric excess for an amino acid ester has also been recently reported.[7] Smaller molecules exhibiting a quinonoid structure constitute a large and important class of organic compounds which display interesting colors and are endowed with very rich chemical and physical properties.[8−10] For years, studies on structure/color relationships have involved *N*-substituted benzoquinonediimines of type **1** (Chart 1) which were only accessible by self-condensation of aniline and/or 1,4-diaminobenzene,[11−13] and this limited considerably the nature of the *N*-substituents on both types of nitrogen atoms. A related system **A** has been envisaged from a theoretical standpoint to contain two 6π-trimethine cyanine subunits linked via two C−C single bonds (Chart 1).[2] However, no experimental data were available to support this description. We recently described a related system **B** which is a rare example of zwitterion being

[†] Laboratoire de Chimie de Coordination.
[‡] Laboratoire de Chimie de Quantique.
[§] Laboratoire DECMET.

(1) Christie, R. M. *Colour Chemistry*; Royal Society of Chemistry: Cambridge, 2001.
(2) Dähne, S.; Leupold, D. *Angew. Chem., Int. Ed. Engl.* **1966**, *5*, 984.
(3) Dähne, S.; Leupold, D.; Radeglia, R. *J. Prakt. Chem.* **1972**, *314*, 525.
(4) König, W. *J. Prakt. Chem.* **1926**, *112*, 1.
(5) Joshi, H. S.; Jamshidi, R.; Tor, Y. *Angew. Chem., Int. Ed.* **1999**, *38*, 2721.
(6) (a) Kraft, A.; Grimsdale, A. C.; Holmes, A. B. *Angew. Chem., Int. Ed.* **1998**, *37*, 403. (b) Noda, T.; Ogawa, H.; Noma, N.; Shirota, Y. *Adv. Mater.* **1997**, *9*, 720.
(7) van Delden, R. A.; Feringa, B. L. *Chem. Commun.* **2002**, 174.
(8) Siri, O.; Braunstein, P. *Chem. Commun.* **2002**, 208.
(9) Bock, H.; Ruppert, K.; Näther, C.; Havlas, Z. *Angew. Chem., Int. Ed. Engl.* **1991**, *30*, 1180.
(10) Pataï, S.; Rappoport, Z. *The Chemistry of the Quinonoid Compounds*; Wiley and Sons: New York, 1988; Vols. 1 and 2.
(11) Bandrowski, E. *Monatsh. Chem.* **1889**, *10*, 123.
(12) Bandrowski, E. *Chem. Ber.* **1894**, *27*, 480.
(13) (a) Fischer, O.; Hepp, E. *Ber. Dtsch. Chem. Ges.* **1888**, *21*, 676. (b) Kimish, C. *Ber. Dtsch. Chem. Ges.* **1875**, *8*, 1026.

Chart 1

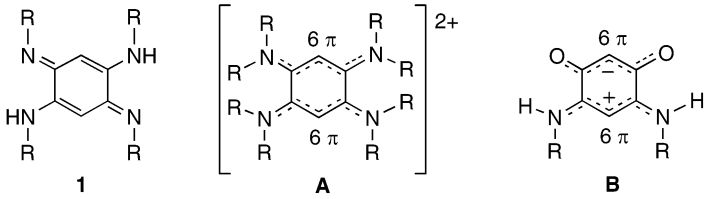

Scheme 1. Synthesis of Compounds **5**−**7**: (*i*) RC(O)Cl/NEt_3/MeCN, (*ii*) $LiAlH_4$/THF, (*iii*) Aerobic Workup

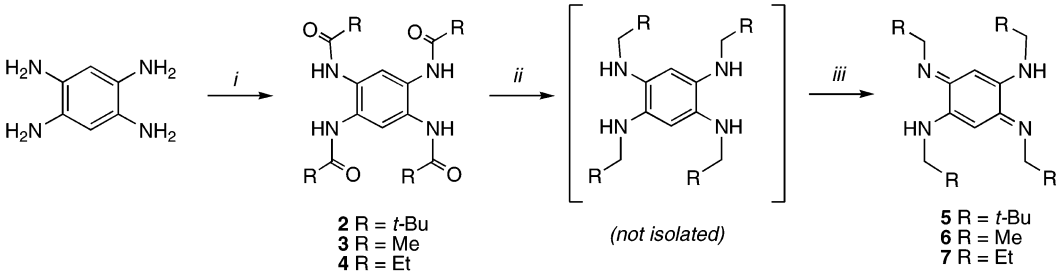

more stable than its canonical forms and which is best described as constituted of two chemically connected but electronically not conjugated 6π-electron subunits.[8,14] A single $\pi \rightarrow \pi^*$ excitation in this 4n π system is sufficient to fully restore π delocalization and antiaromaticity and this has led us to call such systems "potentially antiaromatic".[14] By analogy, we will term 4n π systems such as **A**, **B**, and to some extent **1** "potentially antiaromatic" (see below). In view of the potential of such molecules in color chemistry[15] and as ligands in coordination and organometallic chemistry, we became interested in a simpler and more versatile access to molecules of type **1** bearing *N*-alkyl substituents (instead of the usual and limited aryl groups) whose nature could be more easily varied.[16]

Herein, we report an experimental and theoretical study on a novel family of 12π-electron chromophores based on the 2,5-diamino-1,4-benzoquinonediimine skeleton. These molecules will provide the first experimental evidence for their description as two coupled trimethine cyanine subunits involving 6π electrons each. In this family, the color will be shown to be controlled by successive protonation and depending on the pH, the conjugated localized π electron systems can be tuned to become delocalized. Their electronic structure has been investigated by density functional theory (DFT) calculations. Considering that noncovalent interactions such as hydrogen bonding are essential for the creation of molecular architectures by self-assembly and mutual recognition,[17] our molecules will be shown to have interesting potential as tunable building blocks in supramolecular chemistry for the construction of different types of hydrogen-bonded molecular networks.

Results and Discussion

Synthesis and Characterization. The preparation of *N*,*N*′,*N*″,*N*‴-tetralkyl-*p*-benzoquinonediimine compounds **5**−**7** required the synthesis of the tetraamido derivatives **2**−**4**, which was achieved by condensation reaction between tetraaminobenzene and an appropriate acyl chloride in MeCN and in the presence of excess NEt_3 (Scheme 1).

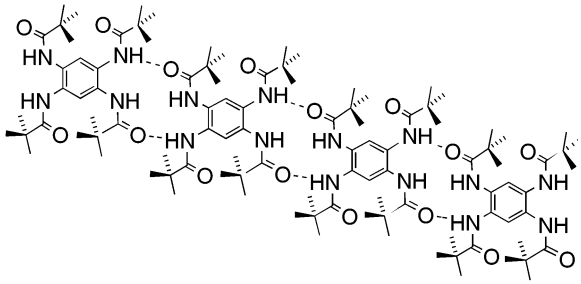

Figure 1. Suggested supramolecular network based on **2**.

Chart 2

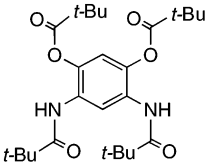

We have recently suggested that the striking insolubility of **2**, which limited its characterization to the solid state,[16] resulted from a H-bonded supramolecular network involving the amido functions,[18,19] as represented in Figure 1. The fact that the diester-diamido analogue (Chart 2) is highly soluble in most organic solvents[8] supports the view that the four amido groups of **2** are involved in this H-bonded network.

The situation is different in the derivatives **3** or **4** which could be dissolved in [d_6]-dmso for NMR characterization. Reduction of **2**−**4** with $LiAlH_4$ in THF followed by aerobic workup afforded the expected *p*-benzoquinonediimine ligands **5**−**7**, respectively. Although the preparation of **3** was mentioned in 1960, its full characterization was not reported.[20] All compounds are stable in the solid state and in solution for several days at room temperature and in the presence of light. Having shown

(14) Braunstein, P.; Siri, O.; Taquet, J.-P.; Rohmer, M.-M.; Bénard, M.; Welter, R. *J. Am. Chem. Soc*. **2003**, *125*, 12246.
(15) Corbett, J. F. *Hair Colorants*: *Chemistry and Toxicology*; Micelle Press: Dorset, England, 1998.
(16) Siri, O.; Braunstein, P. *Chem. Commun*. **2000**, 2223.
(17) Lehn, J. M. *Supramolecular Chemistry*; VCH: Weinheim, 1995.
(18) Hamuro, Y.; Geib, S. J.; Hamilton, A. D. *J. Am. Chem. Soc*. **1996**, *118*, 7529.
(19) Hamuro, Y.; Geib, S. J.; Hamilton, A. D. *J. Am. Chem. Soc*. **1997**, *119*, 10587.
(20) Arient, J.; Marhan, J.; Täublova, H. *Collect. Czech. Chem. Commun*. **1960**, *25*, 1602.

Scheme 2. Protonation Reactions of **5** with HCl

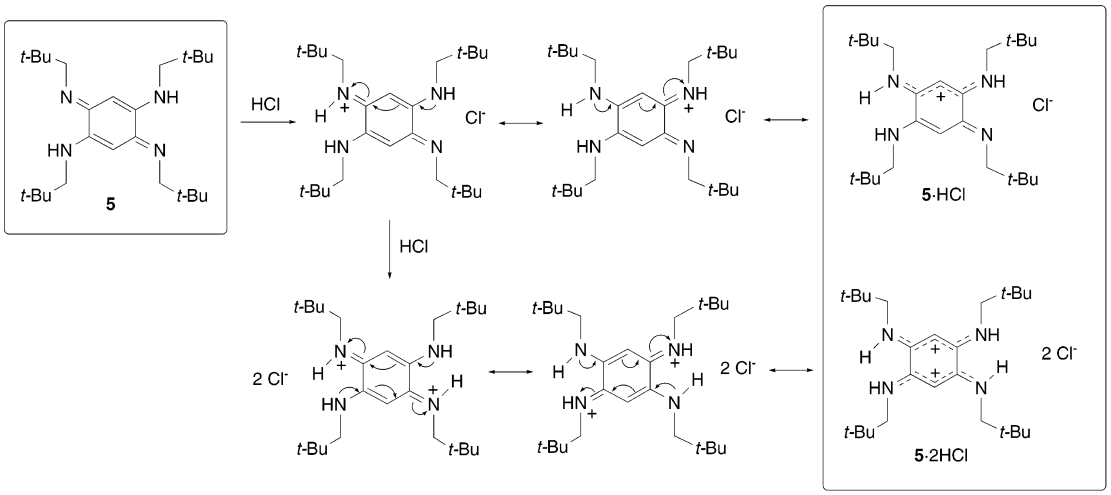

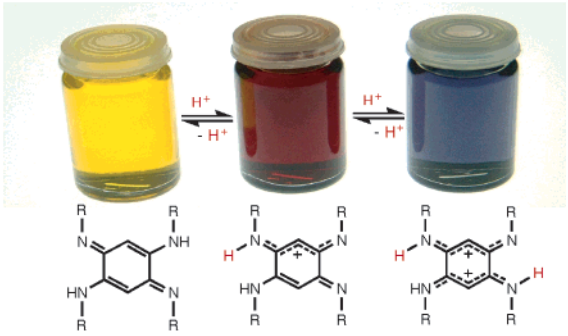

Figure 2. Color changes resulting from mono- and diprotonation of compound **5**.

with **5**−**7** that a general access to *N*-alkyl derivatives of **1** is now available, we will concentrate our detailed studies on **5**.

Influence of pH on Color. The mono- and dicationic compounds derived from **5** were prepared to study the pH color dependence. The successive protonations of **5** were carried out in THF at room temperature with HCl (Scheme 2).

A remarkable color change occurs in solution from yellow for **5** to red for the monoprotonated form **5**·HCl and to blue for the diprotonated form **5**·2HCl (Figure 2).

The UV−visible data will be discussed below. Note that in the solid state, **5**·2HCl is green. These dramatic color changes can be explained by the different electronic situations resulting from protonation at the nitrogen atoms of the imino groups which allows the resulting positive charge to be stabilized by delocalization between the two nitrogen atoms (Scheme 2). Mixing equimolar amounts of **5** and **5**·2HCl in THF afforded quantitatively **5**·HCl. The protonation reaction is reversible upon addition of water or base. All compounds have been fully characterized, including by X-ray diffraction.

Crystal Structures. The molecular structures of compounds **5**·HCl (Figure 3), **5**·2HCl·3$CHCl_3$ (Figure 4), and **5**·HBF_4 have been elucidated by X-ray crystallography. Crystal data and selected bond lengths for **5**·HCl and **5**·2HCl·3$CHCl_3$ are listed in Tables 1 and 2, respectively. The experimental values are compared with those calculated for model compounds in which the neopentyl group has been replaced with H atoms. The results of the theoretical calculations are discussed below. For comparison, we also give in Table 2 relevant structural data for

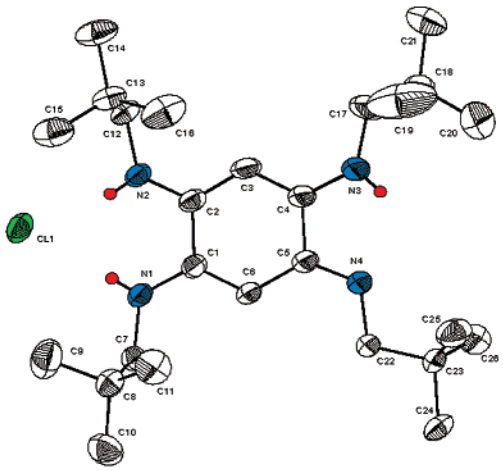

Figure 3. View of the crystal structure of **5**·HCl.

known **5**.[16] Since crystallographic data of **5**·HBF_4 are very similar to those of **5**·HCl, they will not be discussed in detail and are given in the Supporting Information.

Single crystals of **5**·HCl were isolated from a solution of chloroform/*n*-hexane (Figure 3). Examination of the bond distances within the N(1)−C(1)−C(6)−C(5)−N(4) moiety of **5**·HCl reveals an alternating succession of single and double bonds, whereas the C−C and C−N distances of the N(2)−C(2)−C(3)−C(4)−N(3) moiety show a bond equalization (Table 2). The C(1)−C(2) and C(4)−C(5) distances of 1.502(4) and 1.493(4) Å, respectively, correspond to a single bond and indicate the lack of conjugation between the two halves of the molecule. Therefore, **5**·HCl contains in the solid state two different conjugated 6π systems, one *with* and the other *without* delocalization. For the former, the positive charge is shared between the two nitrogen atoms. The intramolecular N(3)H···N(4) hydrogen-bonding distance of 2.036 Å (associated with a C(4)−N(3)−H angle of only 108.5°) is shorter than the N(1)H···N(2) and N(2)H···N(1) distances of 2.412 and 2.335 Å, consistent with the presence of the chloride ion at a distance of 2.265 and 2.172 Å from N(1)H and N(2)H, respectively.

Single crystals of **5**·2HCl·3$CHCl_3$ were isolated from a solution of chloroform/*n*-hexane, and the X-ray analysis revealed (Figure 4) full delocalization of the conjugated π systems as

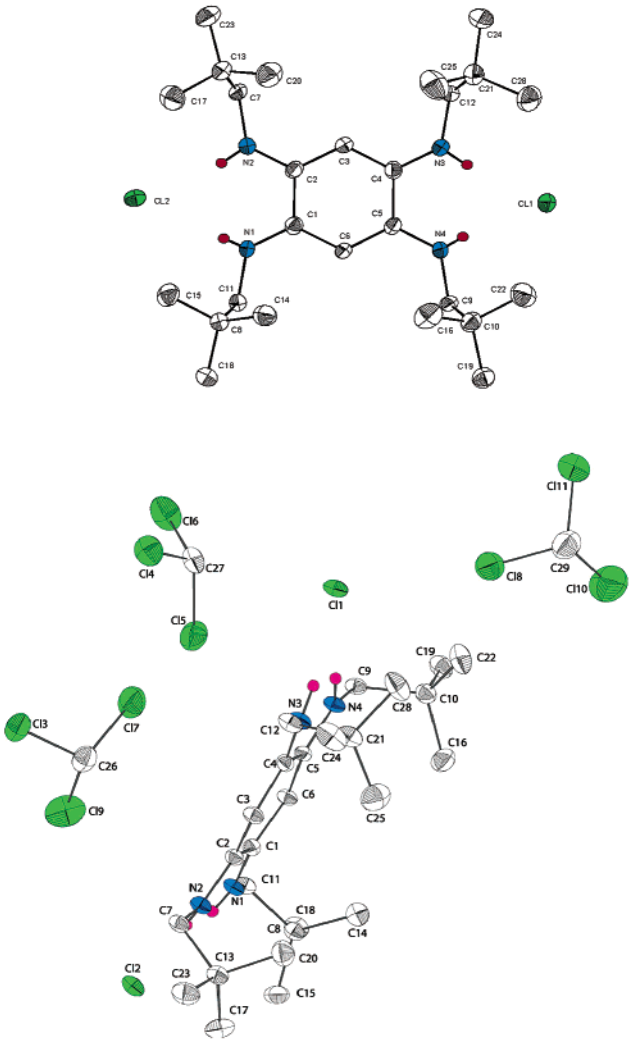

Figure 4. View of the crystal structure of **5**·2HCl in **5**·2HCl·3CHCl$_3$ (top), view of **5**·2HCl·3CHCl$_3$ (bottom).

shown by the narrow range of C−C distances from 1.388(5) to 1.395(5) Å and of C−N distances from 1.316(4) to 1.329(4) Å (Table 2).

The C(1)−C(2) and C(4)−C(5) bond lengths of 1.509(5) and 1.503(5) Å represent typical single bonds and are again indicative of the lack of conjugation between the two halves of the ligand. Delocalization of the π system is therefore confined to the upper and lower parts of the ligand and generates a dicationic benzoquinonediimine-type system with delocalization of each positive charge between the nitrogen atoms. As a result, the dication in **5**·2HCl·3CHCl$_3$ can be regarded as constituted by two cyanine-type chromophores which are mutually connected by two C−C single bonds. The intramolecular N(1)H···N(2) and N(2)H···N(1) hydrogen-bonding distances of 2.528 and 2.374 Å are comparable, respectively, to the N(4)H···N(3) and N(3)H···N(4) distances of 2.447 and 2.367 Å. The Cl(1) chloride ion is at distances of 2.274 and 2.364 Å from N(3)H and N(4)H, respectively, and Cl(2) is at distances of 2.293 and 2.422 Å from N(2)H and N(1)H, respectively. In addition, three $CHCl_3$ molecules cocrystallized and interact with **5**·2HCl by hydrogen bonding via C−H···Cl interactions involving the Cl(5), Cl(7), Cl(8), and Cl(9) atoms (Figure 4).

The bond distances in **5**·HCl and **5**·2HCl·3CHCl$_3$ are similar to those in analogues of quinoxalinophenazine[21] and phenazine[22,23] backbones, respectively, except that in the latter, the bond lengths corresponding to C(1)−C(2) and C(4)−C(5) did not represent a "pure" single bond. Therefore, our molecules constitute the first class of cyanine-type chromophores in which the two "face to face" π systems are fully independent. Compounds **5**·HCl and **5**·2HCl should actually be described as constituted of two chemically connected and interacting, but electronically not conjugated, 6π-electron subunits (see Theoretical Calculations). As established for the related 6π + 6π zwitterion **B** of Chart 1, a single $\pi \rightarrow \pi^*$ excitation from the HOMO to the LUMO would restore the communication between the two π subsystems along with delocalization and antiaromaticity.[14] We have therefore termed such systems "potentially antiaromatic." Since the X-ray analysis of **5** established its *p*-benzoquinonediimine form with no delocalization of the π systems,[16] **5** appears to be the first example of two separated, conjugated, but localized 6π-electron systems that can be tuned by reversible protonation to become delocalized.

Table 1. X-ray Crystallographic Data for **5**·HCl and **5**·2HCl·3CHCl$_3$

	5·HCl	**5**·2HCl·3CHCl$_3$
formula	$C_{26}H_{49}ClN_4$	$C_{29}H_{53}Cl_{11}N_4$
formula weight	453.14	847.70
space group	$P2_1$	$P2_1/n$
a (Å)	11.239(5)	15.060(2)
b (Å)	10.953(5)	14.970(3)
c (Å)	12.182(5)	19.749(3)
α (deg)	90.000(5)	90.000(5)
β (deg)	105.337(5)	108.537(1)
γ (deg)	90.000(5)	90.000(5)
V (Å^3)	1446.2(11)	4221.71(11)
Z	2	4
μ (mm^{-1})	0.150	0.749
ρ (g cm^{-3})	1.041	1.334
θ limits (deg)	$1 < \theta < 30$	$1 < \theta < 27.5$
hkl limits	$-15 \le h \le 15$	$-19 \le h \le 18$
	$-11 \le k \le 15$	$0 \le k \le 19$
	$0 \le l \le 17$	$0 \le l \le 25$
collected reflections	8722	9686
independent reflections (R_{int})	7376	9685
observed reflections ($I > 2\sigma(I)$)	5253	6336
R^a	0.069	0.071
$R_w{}^b$	0.178[c]	0.199[d]
GOF[e]	1.052	1.058
$\Delta\rho_{min}$(e Å^{-3})	−0.38	−1.47
$\Delta\rho_{max}$(e Å^{-3})	0.46	1.77

[a] $R = \sum||F_o| - |F_c||/\sum|F_o|$. [b] $R_w = \{\sum[w(F_o^2 - F_c^2)^2]/\sum[w(F_o^2)^2]\}^{1/2}$. [c] $w = 1/[\sigma^2(F_o^2) + (0.1115P)^2 + 0.0000P]$ where $P = (F_o^2 + 2F_c^2)/3$. [d] $w = 1/[\sigma^2(F_o^2) + (0.1042P)^2 + 2.7829P]$ where $P = (F_o^2 + 2F_c^2)/3$. [e] GOF $= S = \{\sum[w(F_o^2 - F_c^2)^2]/(n - p)\}^{1/2}$ where n is the number of reflections and p is the total number of refined parameters.

Supramolecular Arrangements. Numerous close intermolecular contacts are revealed upon inspection of the crystal lattice in **5**.[16] Two intermolecular C(1)···N(1) distances of 3.998 Å are consistent with intermolecular $\pi-\pi$ interactions (Figure 5).[24]

Depending on the degree of protonation of **5**, different supramolecular architectures are obtained. Thus, **5**·HCl forms a 1-D supramolecular network involving the chloride ion Cl(1) as an intermolecular connector between two molecules. It interacts with the two N−H protons of its associated cation (see

(21) Wudl, F.; Koutentis, P. A.; Weitz, A.; Ma, B.; Strassner, T.; Houk, K. N.; Khan, S. I. *Pure Appl. Chem.* **1999**, *71*, 295.
(22) Ghosh, A. M.; Mitra, K. N.; Mostafa, G.; Goswami, S. *Eur. J. Inorg. Chem.* **2000**, 1961.
(23) Rychlewska, U.; Broom, M. B. H.; Eggleteon, D. S.; Hodgson, D. J. *J. Am. Chem. Soc.* **1985**, *107*, 4768.
(24) Hunter, C. A.; Sanders, J. K. M. *J. Am. Chem. Soc.* **1990**, *112*, 5525.

Table 2. Selected Bond Lengths (Å) Observed for **5**,[16] **5**·HCl, and **5**·2HCl·3CHCl$_3$ and Calculated[a] for Their Respective Models $\mathbf{5_H}$, $\mathbf{5_H}^+$ (optimal and planar), and $\mathbf{5_H}^{++}$ and for the Isolated Fragments HN−(CH)$_3$−NH$_2$ (**11**) and [H$_2$N−(CH)$_3$−(NH$_2$)]$^+$ (**12**$^+$). Labeling of the Atoms: for **5**·HCl and $\mathbf{5_H}^+$, N(2) Is Assumed To Be the Protonated Nitrogen:

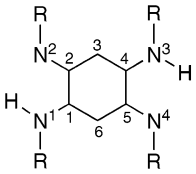

	5	$\mathbf{5_H}$	**5**·HCl	$\mathbf{5_H}^+$ optimal	$\mathbf{5_H}^+$ planar	**5**·2HCl·3CHCl$_3$	$\mathbf{5_H}^{2+}$	**11** planar	**12**$^+$
C(1)−C(2)	1.508(3)	1.502	1.502(4)	1.484	1.488	1.509(5)	1.504		
C(1)−C(6)	1.358(4)	1.370	1.361(4)	1.364	1.372	1.395(5)	1.395	1.360	
C(2)−C(3)	1.437(3)	1.440	1.388(4)	1.396	1.396	1.393(5)	1.395		1.390
C(3)−C(4)	1.358(4)	1.370	1.383(4)	1.394	1.394	1.388(5)	1.395		1.390
C(4)−C(5)	1.508(3)	1.502	1.493(4)	1.508	1.506	1.503(5)	1.504		
C(5)−C(6)	1.437(3)	1.440	1.438(4)	1.446	1.437	1.395(5)	1.395	1.448	
C(4)−N(3)	1.346(3)	1.358	1.338(5)	1.326	1.325	1.318(4)	1.332		1.326
C(1)−N(1)	1.346(3)	1.358	1.368(4)	1.387	1.364	1.316(4)	1.332	1.366	
C(2)−N(2)	1.286(3)	1.303	1.321(3)	1.343	1.344	1.323(4)	1.332		1.326
C(5)−N(4)	1.286(3)	1.303	1.290(4)	1.291	1.294	1.329(4)	1.332	1.292	

[a] With ADF/BP86.

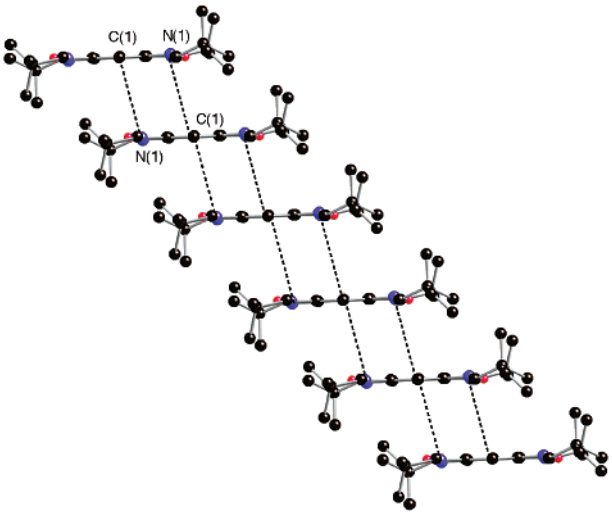

Figure 5. Crystalmaker side view of the stacking of **5** in the solid state. Color coding: nitrogen, blue; hydrogen, red.

above) and a C−H hydrogen of two CH$_2$ groups of another monocationic molecule, as indicated by the C(17)···Cl(1) and C(12)···Cl(1) distances of 3.779 and 3.641 Å, respectively (Figure 6). Therefore, each **5**·HCl unit interacts with two other units. The existence of C−H···Cl hydrogen bonding is now well recognized.[25] A side view of **5**·HCl shows the wavelike arrangement of the H-bonded network (Figure 6, bottom).

In order to study the influence of the nature of the counterion (geometry and/or electronegativity) on the solid-state structure, we prepared **5**·HBF$_4$ and observed the formation of a new H-bonded arrangement (Figure 7). Each monocation interacts with four BF$_4$ anions (three BF$_4$ anions with F···CH$_2$(*t*-Bu) separations in the range 3.391−3.594 Å and one BF$_4$ with F···HN separations of 2.071 and 2.193 Å) which themselves interact with four monocations. Therefore, **5**·HBF$_4$ forms in the solid state a 3-D supramolecular network resulting from the tetrahedral geometry of BF$_4^-$. The bonding parameters are very similar to those for **5**·HCl and are given in the Supporting Information.

(25) Aakeröy, C. B.; Evans, T. A.; Seddon, K. R.; Pálinkó, I. *New J. Chem.* **1999**, 145.

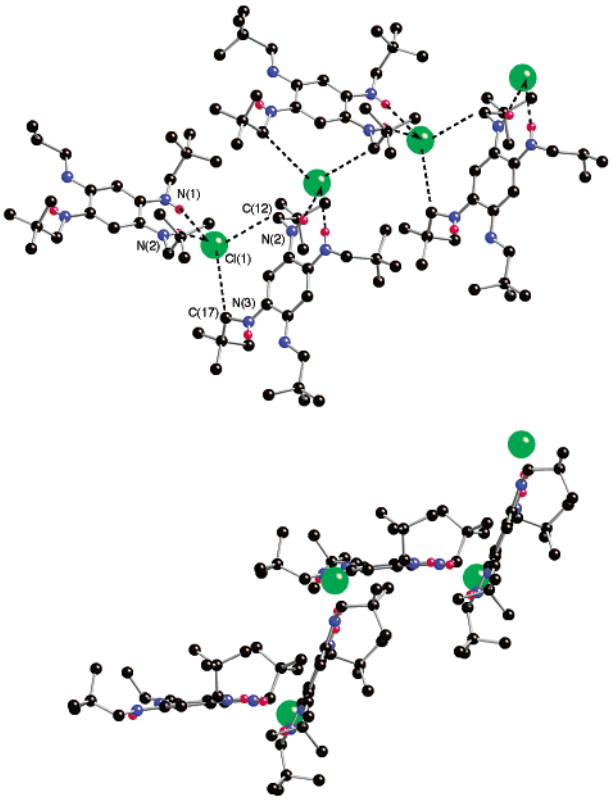

Figure 6. Crystalmaker top and side views of the cation−anion associations in **5**·HCl. Color coding: nitrogen, blue; hydrogen, red; chloride, green.

In **5**·2HCl·3CHCl$_3$, a further step of intermolecular association compared to that of **5**·HCl is achieved through the presence of a second chloride ion on the opposite side of the dication (Figure 4) which generates a 2-D supramolecular network based on C−H···Cl bonding interactions involving now one **5**·2HCl unit in interaction with four other units (Figure 8). Each chloride interacts again with two N−H protons (see above) and a C−H hydrogen of two CH$_2$ groups (four C···Cl distances in the range 3.759−3.845 Å). The Cl anions shown in Figure 8 are coplanar and sandwiched between the planes containing the organic cations, labeled A and B for clarity.

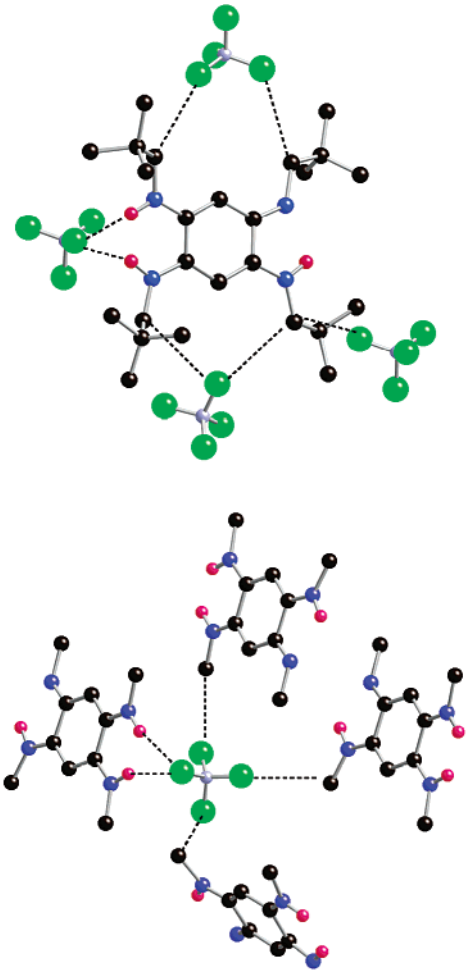

Figure 7. Crystalmaker view of monocation of **5**·HBF_4 interacting with four BF_4^- (top) and BF_4^- interacting with four monocations (bottom, *t*-Bu groups omitted for clarity). Color coding: nitrogen, blue; hydrogen, red; fluoride, green.

Compound **5** can therefore be considered as the parent molecule to a series of salts whose supramolecular architectures in the solid state can be very easily modulated and fine-tuned as a function of the degree of protonation and of the counterion.

NMR Spectroscopy. The ^{1}H NMR data for **5**[16] and its chloride salts are summarized in Table 3. Compound **5** showed only three C−H signals[16] consistent with a fast intramolecular double proton transfer involving two degenerate tautomers generating in solution a structure of higher symmetry (Scheme 3).[26] The detailed mechanism of the related double proton transfer observed in the case of azophenine has been established by kinetic NMR studies.[27]

5·HCl revealed a C_2 symmetry in solution which could be explained similarly by a proton transfer involving two tautomers (Scheme 4). It must be rapid on the ^{1}H NMR timescale since NMR studies carried out at low temperatures did not allow the observation of the two species in solution. Two ^{1}H NMR N−H resonances are observed at $\delta = 9.79$ and 8.20 ppm in a 2:1 ratio, and the two pairs of chemically different CH_2 groups appear as a doublet at $\delta = 3.23$ ppm and a singlet at $\delta = 3.07$ ppm, respectively. The doublet collapses to a singlet upon irradiation of the signal at $\delta = 9.79$ ppm, showing that these protons are mutually coupled and that the resonance at $\delta = 9.79$ ppm corresponds to the N−H not involved in a dynamic process.

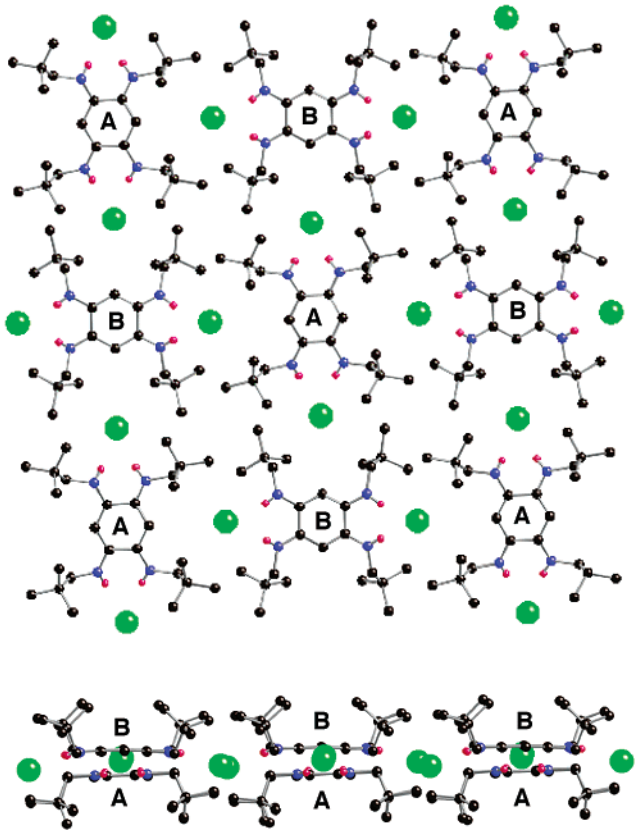

Figure 8. Crystalmaker top and side views of the supramolecular arrangement of **5**·2HCl in the crystal of **5**·2HCl·3$CHCl_3$, illustrating the interactions of each chloride ion with two dications and the almost coplanar arrangement of the chlorides between the A and B layers. Molecules of $CHCl_3$ are omitted for clarity.

Table 3. Comparative ^{1}H NMR Data in $CDCl_3$[a]

solvent		**5**[16]	**5**·HCl	**5**·2HCl
$CDCl_3$	Ha	1.00	1.01(s) 1.09(s)	1.12
	Hb	2.95	3.07(s) 3.23(d)	3.37
	Hc	5.16	5.38	5.63
	NH	6.75	8.20 9.79	11.92

[a] H codes: Ha (*t*-Bu protons), Hb (CH_2 protons), Hc (olefinic protons).

Scheme 3. Tautomeric Equilibrium of **5** in Solution

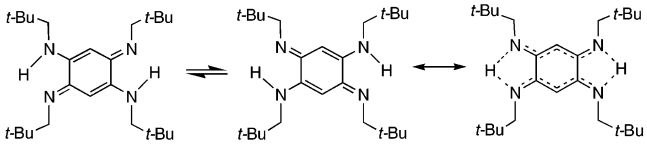

Scheme 4. Tautomeric Equilibrium of **5**·HCl in Solution

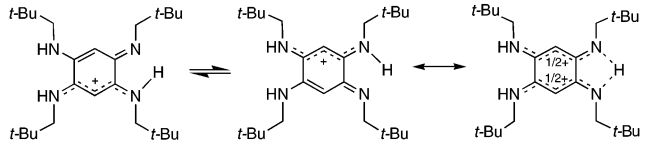

(26) For recent results on double proton transfer in N−H···O and N···H−O systems, see: Osmialowski, B.; Kolehmainen, E.; Gawinecki, R. *Chem. Eur. J.* **2003**, *9*, 2710.
(27) Rumpel, H.; Limbach, H.-H. *J. Am. Chem. Soc.* **1989**, *111*, 5429.

Table 4. Spectroscopic Data in CH_2Cl_2 of **5** and Its Protonated Forms (relative intensities)

	5	**5**·HCl	**5**·2HCl
λ (nm)	340(br) (1.0) 426(br) ($<10^{-3}$)	372(br) (1.0) 527(br) ($<10^{-3}$)	374(br) (1.0) 564(br) ($<10^{-3}$)

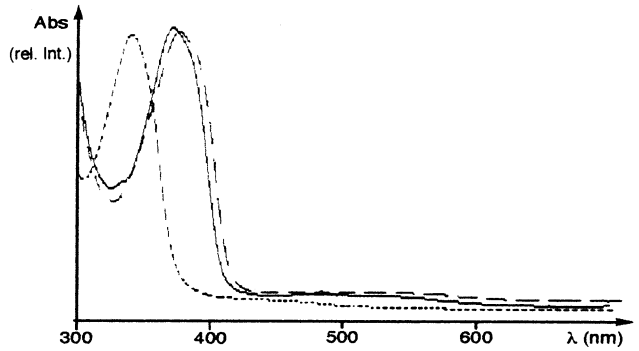

Figure 9. UV−vis spectra in CH_2Cl_2 of **5**(- - -), **5**·HCl (—), and **5**·2HCl (— —).

The cation of **5**·2HCl shows a D_{2h} symmetry in solution which is consistent with the protonation of both imino groups of **5** inducing the electronic delocalization of the two positive charges between the nitrogen atoms (Scheme 2). The four N−H protons are shifted downfield ($\delta = 11.92$ ppm) with respect to **5**·HCl because of the lower electronic density due to the presence of two positive charges.

As expected, the NMR resonances for the protonated forms are shifted downfield from those for the neutral parent **5**. The olefinic protons shift from $\delta = 5.16$ for **5** to 5.38 ppm for **5**·HCl and to 5.63 ppm for **5**·2HCl in $CDCl_3$, which is consistent with the increase of the positive charge density on the corresponding C−H carbon atom.

UV Absorption Spectroscopy. Compounds **5**−**7** show intense absorption bands approximately at 340 nm that are assigned to the intraquinone transitions of the ligands.[10] The absorption wavelength is therefore only slightly influenced by the nature of R, at least when R is an alkyl group. In contrast, the color can be modulated by exogenous additives such as a metal ion. Indeed, we recently reported the color change from yellow to green in the diplatinum derivative **10**,[16] and this prompted us to study the influence of the simplest electrophile, the proton, on the color change (Figure 2 and Table 4).

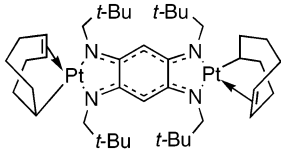

10

Compounds **5**·HCl and **5**·2HCl display a broad, intense absorption band at 372 and 374 nm, respectively, which can be assigned to the intraquinone transition (Figure 9).

Each compound revealed an additional, very weak absorption (Table 4).

The pronounced red shift of the intraquinone transition absorption of **5**·HCl and **5**·2HCl with respect to **5** ($\lambda_{max} =$ 340 nm) may result from the delocalization of the conjugated π system. Similarly, organic conjugated chromophores with more π delocalization exhibit a more cyanine-like character.[28,29]

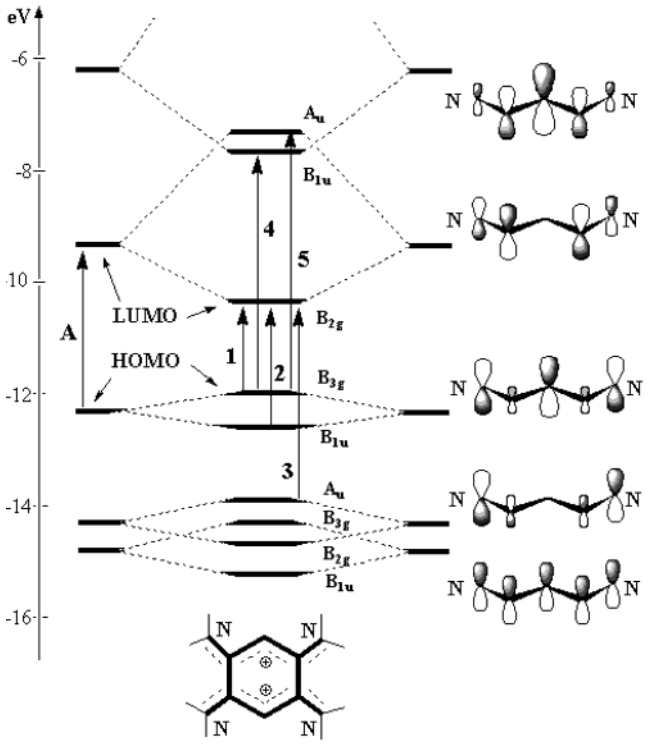

Figure 10. Orbital interaction diagram obtained for the model of **5**·2HCl by means of EHT calculations.

To gain more insight into the relation between the electronic spectrum and the π-electron delocalization (or not) of our systems, theoretical calculations were performed on **5**, **5**·HCl, and **5**·2HCl.

Theoretical Calculations. Geometry optimizations have been carried out at the DFT level on models of **5**, **5**·HCl, and **5**·2HCl, respectively referred to as $\mathbf{5_H}$, $\mathbf{5_H}^+$, and $\mathbf{5_H}^{++}$ in which the four neopentyl substituents have been replaced by hydrogens. The calculated distances are displayed in Table 2. The maximal discrepancy with respect to the distances observed in the real molecules is equal to 0.022 Å (C(2)−N(2) distance in the monoprotonated system). The neutral molecule has a fully quinonic structure with a marked alternation of short and long bonds throughout both N−C−C−C−N moieties. Conversely, both moieties are fully delocalized in the diprotonated molecule, but the communication between the two 6π subsystems is interrupted by two long C(1)−C(2) and C(4)−C(5) bonds, both longer than 1.5 Å, with very little π character. In fact, the π MOs of $\mathbf{5_H}$ and its protonated derivatives can be deduced from an interaction diagram between the π orbitals of two $[H_2N-(CH)_3-NH_2]^{n+}$ fragments ($n = 0,1$), as displayed in Figure 10 for $\mathbf{5_H}^{++}$. Since the two π subsystems are forced to approach each other because of the σ framework, the orbitals do overlap and split into a stabilized bonding level and its antibonding counterpart. But despite this interaction, the two π subsystems basically remain separated in the molecular ground state, since both the bonding *and* the antibonding terms of each interacting couple are either doubly occupied or unoccupied. Each π-bonding contribution is therefore canceled by its antibonding

(28) Bourhill, G.; Brédas, J.-L.; Cheng, L.-T.; Marder, S. R.; Meyers, F.; Perry, J. W.; Tiemann, B. G. *J. Am. Chem. Soc.* **1994**, *116*, 2619.
(29) Gorman, C. B.; Marder, S. R. *Proc. Natl. Acad. Sci. U.S.A.* **1993**, *90*, 11297.

counterpart.[30] The diagram of Figure 10 summarizes the "coupling principles" formulated 35 years ago by Dähne and Leupold to assign the visible spectrum of organic dyes,[2] and the Kohn−Sham orbitals obtained for the ground state of the 12π-electron systems studied in the present work match these principles. Qualitatively similar diagrams involving one or two nonsymmetric fragments could indeed be obtained for $\mathbf{5_H}^+$ and for $\mathbf{5_H}$, respectively. In the monoprotonated molecule, the N(2)−C(2)−C(3)−C(4)−N(3) moiety appears quite delocalized, whereas the neutral fragment displays bond length alternation. An important difference between the protonated molecules considered isolated or in the crystal concerns the pyramidality at nitrogen N(1) (Figure 3). The sum of the angles at N(1) in the optimized geometry of the $\mathbf{5_H}^+$ model amounts to 342°, which corresponds to a pronounced pyramidality. For comparaison, the sum of the angles calculated at N(2) and N(3), in the delocalized part, is close to 357°, with experimental values of 359.8 and 359.5°, respectively. Since no such trend toward pyramidality is calculated either at the NH_2 groups of $\mathbf{5_H}$ (sum of the experimental angles around N(1) in **5**: 357.5°) or at that of the isolated fragment HN−$(CH)_3$−NH_2 (**11**), the weakening of the C═N double bond character in the quinonic structure is probably not sufficient to induce an umbrella folding at N. We expect the H···H nonbonding contact (2.12 Å) between the closest hydrogens of the neighboring NH_2 groups to activate the trend toward pyramidality of the weakly conjugated nitrogen. This trend is, however, not observed in the crystal structure of **5**·HCl where deviations from planarity do not exceed 0.2 Å (sum of the angles at N(1) = 359.8°). This difference could be due to the influence of the adjacent counterion (Figure 3) or to the presence of the alkyl substituent in the real molecule. An optimization of $\mathbf{5_H}^+$ with a constraint of complete planarity yielded a destabilization of 1.9 kcal.mol^{-1}. In the planar form, the calculated C(1)−N(1) distance is reduced from 1.387 to 1.364 Å, in better agreement with experiment (1.368 Å), and the amplitude of the bond alternation in the quinonic fragment is somewhat decreased (Table 2), with practically no change in the delocalized part. Note that the amplitude of the C−C bond alternation in the localized moiety of planar $\mathbf{5_H}^+$ (1.372 Å/1.437 Å) is slightly lower than in the isolated fragment HN−$(CH)_3$−NH_2 (**11**) (1.360 Å/1.448 Å), suggesting a residual influence of the delocalized fragment on the π system.

The coupling principles formulated first by Dähne and Leupold can also be used to assign the $\pi \rightarrow \pi^*$ transitions of **5**, **5**·HCl, and **5**·2HCl. According to Dähne and Leupold,[2] organic dyes are composed of several polymethine structural units of the type X−$(CR)_n$−X′, with n odd and X and X′ being heterosubstituents. The π system of such units is generally composed of $p + 1$ (sometimes $p - 1$) electrons, p being the number of chain atoms. Compounds **5**, **5**·HCl, and **5**·2HCl meet this definition since they are composed of two polymethine units corresponding to $n = 3$, $p = 5$, and generating each 6π electrons. Although each polymethine unit remains basically unaltered because of the lack of interunit π delocalization, the π orbitals of the isolated units are split in the resulting molecule in proportion to their overlap. Each level of the isolated 6π system generates in $\mathbf{5_H}$ or in its cations a stabilized, in-phase orbital and a destabilized, out-of-phase MO. A good overview of the π MOs in **5**·2HCl can therefore be obtained from an orbital interaction diagram between the π levels of two [H_2N−$(CH)_3$−NH_2)]$^+$ fragments. This diagram obtained from extended Hückel calculations is displayed in Figure 10.

The orbital splitting will be mainly controlled by the coefficient of the π orbital on the terminal carbons of the fragment. This coefficient is large in the two fragment π-unoccupied orbitals, which generates an important splitting. It is much reduced in the set of three occupied fragment orbitals; the splitting is relatively small and all of the six resulting MOs are close in energy. That is why the two $\pi \rightarrow \pi^*$ transitions of the visible spectrum and some of those in the near UV result from a transition to the molecular LUMO. The molecular levels have been labeled according to point group D_{2h}, to which belongs $\mathbf{5_H}^{++}$, the model of the dication. According to the symmetry selection rules, the HOMO−LUMO transition, labeled **1** in Figure 10, should be forbidden, whereas transitions labeled **2**−**5** should be allowed.

Although the diagram of Figure 10 generates the orbitals of the fully symmetric $\mathbf{5_H}^{++}$ dication, it can also be used to assign the $\pi \rightarrow \pi^*$ transitions of **5** and **5**·HCl. The π orbitals of the neutral HN−$(CH)_3$−NH_2 fragment are basically similar in shape and in energy to those of [H_2N−$(CH)_3$−NH_2]$^+$ despite a slight deviation from C_{2v} symmetry. The symmetry of the resulting molecule is therefore lowered to C_i for $\mathbf{5_H}$ (allowing for a slight out-of-plane distortion of ±0.12 Å on hydrogens), and to C_s for $\mathbf{5_H}^+$, assumed planar. In the latter case only, the HOMO → LUMO transition becomes formally allowed, but the oscillator strength remains weak, as can be expected (Table 5).

The lowest excitation energies of $\mathbf{5_H}$, $\mathbf{5_H}^+$, and $\mathbf{5_H}^{++}$ and those of fragments **11** and $\mathbf{12}^+$ (see Table 2) have been calculated using the TD-DFT formalism[31−34] as implemented in ADF and in Gaussian 98 (See Computational Details). The computed energies and oscillator strengths are displayed in Table 5. It is important to recall that the assignment of the $\pi \rightarrow \pi^*$ excitations in terms of the orbital-to-orbital scheme of Figure 10 represents an approximation, since each excited state should be properly described in terms of a combination of occupied-to-virtual contributions of same symmetry. The proposed assignment refers to the contributions with highest weight.

An interesting trend can be deduced from the HOMO → LUMO excitation energy in fragments **11** and $\mathbf{12}^+$. In the nonsymmetric, neutral fragment, this lowest $\pi \rightarrow \pi^*$ transition has its highest weight (55%) in an excited-state calculated at 5.40 eV (230 nm). The energy of the lowest $\pi \rightarrow \pi^*$ excited state in the *cationic fragment*, which mainly corresponds to the same HOMO → LUMO excitation, is significantly decreased at 5.21 eV (238 nm). The replacement of **11** by $\mathbf{12}^+$ which occurs once for $\mathbf{5_H}^+$ and twice for $\mathbf{5_H}^{++}$ therefore explains the bathochromic trend observed upon protonation for the two lowest $\pi \rightarrow \pi^*$ excitations (Table 5).

Excitation energies calculated with the hybrid B3LYP functional are larger by 0.25−0.8 eV than those calculated with BP86, and oscillator strengths are systematically lower. How-

(30) The interaction between the π subsystems can be compared to that occurring between two atoms of rare gas forced to approach each other. Atomic levels are split by the interaction generating Pauli repulsion, but with no bond and no electron delocalization.

(31) ADF user's guide; Theoretical Chemistry Department, Vrije Universiteit, Amsterdam, The Netherlands, 1999.
(32) Baerends, E. J.; Ellis, D. E.; Ros, P. *Chem. Phys.* **1973**, *2*, 41.
(33) Te Velde, G.; Baerends, E. J. *J. Comput. Phys.* **1992**, *99*, 84.
(34) Fonseca-Guerra, C.; Visser, O.; Snijders, J. G.; Te Velde, G.; Baerends, E. J. In *Methods and Techniques in Computational Chemistry*: *METECC-95*; Clementi E.; Corongiu, G., Eds.; STEF: Cagliari, Italy, 1995; p 305.

Table 5. Relative Energies (nm) and Oscillator Strengths (*f*, dimensionless) Calculated[a] for the Lowest-Excited States of **11**, **12**$^+$, **5$_H$**, **5$_H$**$^+$, and **5$_H$**$^{++}$ [b]

	ADF/BP86			Gaussian/B3LYP		assignment		experiment[c]
	sym	energy	*f*[d]	energy	*f*	type	weight[e]	λ_{max} (nm)
11 (C_s)	*A′*	230	0.47	220	0.10	$\pi \rightarrow \pi^*$	55	
12$^+$ (C_{2v})	B_2	238	0.71	231	0.10	$\pi \rightarrow \pi^*$	98	
5$_H$ (C_i)	A_g	511	0	427	0	**1**	98	426
	A_u	353	0.20	307	0.04	**2**	81	340
	A_g	331	0	289	0	$n \rightarrow \pi^*$	100	
	A_u	318	0.003	277	0.0006	$n \rightarrow \pi^*$	99	
	A_u	251	0.14	214	0.03	**4**	43	
						3	34	
5$_H$ $^+$ (C_s)[f]	*A′*	613	0.01	519	0.001	**1**	97	527
	A″	407	0.001	352	0.0002	$n \rightarrow \pi^*$	100	
	A′	359	0.17	316	0.03	**2**	86	372
	A′	265	0.09	228	0.02	**4**	45	
						3	41	
	A′	245	0.03	217	0.005	**3**	50	
						4	37	
	A′	206	0.59	194	0.13	**5**	66	
5$_H$ $^{++}$ (D_{2h})	B_{1g}	682	0	602	0	**1**	98	564
	B_{3u}	396	0.18	351	0.03	**2**	83	374
	B_{2u}	247	0.17	217	0.04	**3**	66	
						4	31	
	B_{2u}	230	0.004	207	0.0002	**3**	31	
						4	65	
	B_{3u}	208	1.02	198	0.17	**5**	83	

[a] With respect to the ground-state energy. The reported results have been obtained using the TD-DFT formalism with ADF/BP86 and Gaussian/B3LYP. [b] Assignments are proposed on the basis of the occupied-to-virtual excitation with highest weight. The $\pi \rightarrow \pi^*$ excited states follow the numbering of Figure 10. [c] In CH_2Cl_2 (See Table 4). [d] A forbidden transition is indicated by 0. [e] In %, from ADF calculations. [f] Assumed to be planar.

ever, the sequence of states and the energy differences are quite similar and allow a reliable assignment of the experimental spectrum. In **5$_H$** as in the two cationic systems, the lowest excited state originates from the HOMO → LUMO excitation, which is forbidden by symmetry in **5$_H$** and **5$_H$**$^{++}$ and allowed with a weak oscillator strength in **5$_H$**$^+$. The red shift calculated from **5$_H$** to **5$_H$**$^+$ (∼100 nm) and then to **5$_H$**$^{++}$ (70−80 nm) parallels the observed displacement of the weak band from $\lambda_{max} = 426$ nm for **5** to $\lambda_{max} = 564$ nm for **5**·2HCl (Table 5). The intense band of the experimental spectra is assigned to a $\pi \rightarrow \pi^*$ excitation, the major component of which is the HOMO−1 → LUMO transition. A significant red shift is also observed for this band upon protonation (34 nm from **5** to **5**·2HCl), but the calculated shift is more pronounced for the second protonation process, at variance with experiment. The two nitrogen lone pairs of **5** and the single one remaining in **5**·HCl should generate as many low-energy n → π^* transitions. Calculations locate these transitions about 20 and 30−35 nm beyond the intense band for **5$_H$**, but one-electron protonation shifts the n → π^* transition to low energies by ∼70 nm, leading for **5$_H$**$^+$ to an inversion of the relative ordering with respect to the intense $\pi \rightarrow \pi^*$ transition. When allowed by symmetry, the n → π^* transitions are characterized by a very low oscillator strength, and their detection in this part of the spectrum should prove difficult. The occurrence of two $\pi \rightarrow \pi^*$ excitations is then predicted in the region 250−230 nm. These excitations are allowed, with an intensity globally similar to that of the band observed in the region 370−340 nm. Both excitations are assigned to a mixture between HOMO−2 → LUMO and HOMO → LUMO+1 transitions (Table 5). It should be noted that these two $\pi \rightarrow \pi^*$ excitations are not internal to the set of four levels stemming from the splitting of the frontier orbitals in fragments **11** and **12**$^+$ (Figure 10). The second excitation allowed by symmetry within this orbital set, namely the HOMO → LUMO+2 is the main contributor to a very intense band predicted to appear around 200 nm.

Conclusion

In this article, we have presented a novel family of "potentially antiaromatic" alkyl-substituted *p*-benzoquinonediimine ligands of type **1**. We have shown that these 12π-electron molecules should be better considered as constituted by two chemically connected but electronically not conjugated 6π-electron subunits. Molecule **5** appears to be the first example of two separated, conjugated, but localized, 6π-electron systems that can be tuned by reversible protonation to become delocalized. The mono- and diprotonated derivatives have been characterized by spectroscopic methods and X-ray diffraction. These systems form supramolecular arrangements in the solid state that clearly reflect the degree of protonation and depend on the nature of the counterion. These compounds constitute new chromophores for which the color can be tuned depending on the degree of protonation, going in solution from yellow for **5** to red for **5**·HCl and blue for **5**·2HCl. Theoretical calculations have provided a deeper insight into the electronic structure of these molecules and allowed an assignment of the experimental UV−vis spectra. The visible and near-UV spectrum of the neutral and protonated benzoquinonediimines can be classically assigned from the coupling of two 6π-electron polymethine units. TD-DFT calculations confirm the observed red shift of the two lowest $\pi \rightarrow \pi^*$ transitions of the benzoquinonediimines upon protonation and relate it to the moderate energy lowering of the HOMO → LUMO transition induced by the delocalization of the polymethine π system. The protonation-dependent behavior of these molecules has prompted us to examine the use of such molecules as sensors in the detection of protons, including in biocompatible media, and the results will be presented elsewhere.[35] The obvious potential of these new ligands in inorganic chemistry and homogeneous catalysis is also being explored.

Experimental Section

Commercial analytical-grade reagents were obtained from commercial suppliers and were used directly without further purification. Solvents were distilled under argon prior to use and dried by standard methods. ^{1}H NMR spectra were recorded in $CDCl_3$ and [d_6]-dmso with a AC300 Bruker spectrometer, operating at 300 MHz for ^{1}H spectra. Chemical shifts are reported in δ units, in parts per million (ppm) relative to the singlet at $\delta = 7.26$ for $CDCl_3$. Splitting patterns are designated as s, singlet; d, doublet; t, triplet; q, quartet; sext, sextuplet; m, multiplet; br, broad. Elemental analyses were performed by the service de Microanalyse de l'Institut de Chimie, Strasbourg. FAB mass spectral analyses were recorded on an autospec HF mass spectrometer, and EI mass spectral analyses were recorded on a Finnigan TSQ 700.

Synthesis. *1,2,4,5*-Tetraacetamidobenzene (3). Similarly to the procedure described for the synthesis of **2**[16] but using THF as a solvent, tetraminobenzene tetrahydrochloride (500 mg, 1.76 mmol) was reacted

(35) Elhabiri, M.; Siri, O.; Sornosa-Tent, A.; Albrecht-Gary, A.-M.; Braunstein, P. *Chem. Eur. J.*, in press.

with acetyl chloride (553 mg, 7.04 mmol), and **3** was obtained as a white solid (110 mg, 20%). ^{1}H NMR (300 MHz, [d_6]-dmso): δ = 2.05 (s, 12 H, CH_3), 7.74 (s, 2 H, H_{arom}), 9.32 (br s, 4 H, NH); MS (40 eV, EI): m/z = 306.2 $[M]^+$. Anal. Calcd for $C_{14}H_{18}N_4O_4$: C, 54.89; H, 5.92; N, 18.29. Found: C, 54.09; H, 5.88; N, 18.05.

***1,2,4,5*-Tetrapropylamidobenzene (4).** Similarly, tetraminobenzene tetrahydrochloride (500 mg, 1.76 mmol) was reacted with propanoyl chloride (651 mg, 7.04 mmol), and **4** was obtained as a white solid (223 mg, 35%). ^{1}H NMR (300 MHz, [d_6]-dmso): δ = 1.08 (t, $^3J_{HH}$ = 7.5 Hz, 12 H, CH_3), 2.33 (q, $^3J_{HH}$ = 7.5 Hz, 8 H, CH_2), 7.70 (s, 2 H, H_{arom}), 9.24 (s, 4 H, NH); MS (40 eV, EI): m/z = 362.3 $[M]^+$. Anal. Calcd for $C_{18}H_{26}N_4O_4$: C, 59.65; H, 7.23; N, 15.46. Found: C, 59.42; H, 7.16; N, 15.39.

General Procedure for the Synthesis of 5·HX. To a solution of **5** dissolved in THF (50 mL) were added a few drops of diluted HX (50/50 v/v) until the color changed from yellow to deep red. The solution was stirred at room temperature for 10 min. After evaporation to dryness under reduced pressure, the residue was suspended in Et_2O. Filtration of the insoluble red solid afforded **5**·HX.

Synthesis of 5·HCl. Route A. As described above in the general procedure, **5**·HCl was obtained as a red solid (0.121 g, 75%). ^{1}H NMR (300 MHz, $CDCl_3$): δ = 1.01 (s, 18 H, CH_3), 1.09 (s, 18 H, CH_3), 3.07 (s, 4 H, CH_2), 3.23 (d, $^3J_{HH}$ = 6.0 Hz, 4 H, CH_2), 5.38 (s, 2 H, $H_{olefinic}$), 8.20 (br s, 1 H, NH), 9.79 (br s, 2 H, NH). Anal. Calcd for $C_{26}H_{49}ClN_4$: C, 68.91; H, 10.90; N, 12.36. Found: C, 68.46; H, 11.18; N, 12.08.

Route B. To a blue solution of **5**·2HCl (prepared as detailed below) dissolved in THF (50 mL) was added a yellow solution of **5** dissolved in THF (20 mL). The color of the solution turned red. The solution was stirred at room temperature, and after 10 min, the solvent was evaporated under reduced pressure. The residue was taken up in Et_2O, and the insoluble red suspension was filtered, affording quantitatively **5**·HCl.

Synthesis of 5·HBF$_4$. Using the general procedure, we similarly obtained **5**·HBF_4 as a red solid (0.148 g, 68%). ^{1}H NMR (300 MHz, $CDCl_3$): δ = 1.03 (s, 18 H, CH_3), 1.06 (s, 18 H, CH_3), 3.14 (s, 4 H, CH_2), 3.20 (d, $^3J_{HH}$ = 5.6 Hz, 4 H, CH_2), 5.50 (s, 2 H, $H_{olefinic}$), 7.06 (br s, 2 H, NH), 8.29 (br s, 1 H, NH). Anal. Calcd for $C_{26}H_{49}BF_4N_4$: C, 61.90; H, 9.79; N 11.11. Found: C, 61.43; H, 9.77; N, 11.09.

Synthesis of 5·2HCl. To a solution of **5** dissolved in THF (50 mL) was added dropwise a large excess of HCl 12N (0.25 mL). The solution was stirred at room temperature for 10 min. The precipitate was then collected by filtration as a blue solid (0.133 g, 66%). ^{1}H NMR (300 MHz, $CDCl_3$): δ = 1.12 (s, 36 H, CH_3), 3.37 (s, 8 H, CH_2), 5.63 (s, 2 H, $H_{olefinic}$), 11.92 (br s, 4 H, NH). Anal. Calcd for $C_{26}H_{50}Cl_2N_4$: C, 63.78; H, 10.29; N, 11.44. Found: C, 62.66; H, 10.36; N, 11.24.

***N,N′,N″,N‴*-Tetraethyl-*p*-benzoquinonediimine (6).** Similarly to the procedure described for the synthesis of **5**,[16] **3** (110 mg, 0.359 mmol) was reduced with $LiAlH_4$, and **6** was obtained as a yellow solid (35 mg, 39%). ^{1}H NMR (300 MHz, $CDCl_3$): δ = 1.28 (t, $^3J_{HH}$ = 7.5 Hz, 12 H, CH_3), 3.27 (q, $^3J_{HH}$ = 7.5 Hz, 8 H, CH_2), 5.22 (s, 2 H, $H_{olefinic}$), 6.75 (br s, 2 H, NH); MS (40 eV, EI): m/z = 248.3 $[M]^+$. Anal. Calcd for $C_{14}H_{24}N_4$: C, 67.70; H, 9.74; N, 22.56. Found: C, 67.12; H, 9.64; N, 22.41. UV−vis (CH_2Cl_2): λ_{max} = 339 nm [ϵ = 26400 mol^{-1} dm^3 cm^{-1}].

***N,N′,N″,N‴*-Tetrapropyl-*p*-benzoquinonediimine (7).** Similarly, **4** (223 mg, 0.615 mmol) was reduced with $LiAlH_4$, and **7** was obtained as an orange solid (109 mg, 58%). ^{1}H NMR (300 MHz, $CDCl_3$): δ = 0.99 (t, $^3J_{HH}$ = 7.5 Hz, 12 H, CH_3), 1.70 (sext, $^3J_{HH}$ = 7.5 Hz, 8 H, CH_3-CH_2), 3.20 (br s, 8 H, $N-CH_2$), 5.22 (s, 2 H, $H_{olefinic}$), 6.35 (br s, 2 H, NH); MS (40 eV, EI): m/z = 304.5 $[M]^+$. Anal. Calcd for $C_{18}H_{32}N_4$: C, 71.01; H, 10.59; N, 18.40. Found: C, 70.42; H, 10.65; N, 17.94. UV−vis (CH_2Cl_2): λ_{max} = 339 nm [ϵ = 26800 mol^{-1} dm^3 cm^{-1}].

Computational Details. DFT calculations have been carried out on models of **5**, **5**·HCl, and **5**·2HCl in which the four neopentyl substituents have been replaced by hydrogens. These model molecules, respectively referred to as $\mathbf{5_H}$, $\mathbf{5_H}^+$, and $\mathbf{5_H}^{++}$, have been optimized within the framework of the Generalized Gradient Approximation (GGA), as implemented in the ADF program[31−34] with the so-called BP86 exchange-correlation functional.[36,37] The 1s shell of carbon and nitrogen was frozen and described by a single Slater function. The valence shells were described by triple-ζ Slater orbitals and supplemented with one polarization function.[38,39] Molecular bonding energies are reported with respect to an assembly of neutral atoms assumed isolated and in their ground state. Geometry optimizations have been carried out with the following symmetry constraints: C_{2h} for $\mathbf{5_H}$, C_1 for $\mathbf{5_H}^+$, C_{2v} for $\mathbf{5_H}^{++}$. Planarity was then assumed for $\mathbf{5_H}^+$ and $\mathbf{5_H}^{++}$. The optimization cycles were continued until all of the three following convergence criteria were fulfilled: (i) the difference in the *total energy* between two successive cycles is less than 0.001 hartree; (ii) the difference in the *norm of the gradient* between two successive cycles is less than 0.001 hartree·Å^{-1}; (iii) the maximal difference in the *Cartesian coordinates* between two successive cycles is less than 0.01 Å. The energies of the lowest excited states have then been calculated using the TD-DFT formalism,[40] as implemented in ADF and using the same BP86 exchange-correlation functional. To test the influence of the exchange-correlation functional on the calculated excitation energies, the TD-DFT formalism was applied again to all three model systems using the hybrid B3LYP functional, the all-electron 6-31G** set of basis functions for all atoms, and reoptimized geometries. These calculations were carried out with *Gaussian 98*.[41−43]

X-ray Data. Selected crystals were mounted on a Nonius Kappa-CCD area detector diffractometer (Mo Kα, λ = 0.71073 Å). The complete conditions of data collection (Denzo software) and structure refinements are given in Table 1. The cell parameters were determined from reflections taken from one set of 10 frames (1.0° steps in phi angle), each at 20 s exposure. The structures were solved using direct methods (SIR97) and refined against F^2 using the SHELXL97 software. The absorption was not corrected. All nonhydrogen atoms were refined anisotropically. Hydrogen atoms were generated according to stereochemistry and refined using a riding model in SHELXL97.[44]

Acknowledgment. We gratefully acknowledge support of this research by the Centre National de la Recherche Scientifique

(36) Perdew, J. P. *Phys. Rev.* **1986**, *B34*, 7406.
(37) Becke, A. D. *Phys. Rev.* **1988**, *A38*, 3098.
(38) Snijders, J. G.; Baerends, E. J.; Vernooijs, P. *At. Nucl. Tables* **1982**, *26*, 483.
(39) Vernooijs, P.; Snijders, J. G.; Baerends, E. J. *Slater type basis functions for the whole periodic system* (Internal Report); Free University of Amsterdam: The Netherlands, 1981.
(40) Casida M. E. In *Recent Developments of Modern Density Functional Theory*; Seminario, J. M., Ed.; Theoretical and Computational Chemistry, Vol. 4; Elsevier: Oxford, 1996, p 391.
(41) Stratmann, R. E.; Scuseria, G. E.; Frisch, M. J. *J. Chem. Phys.* **1988**, *109*, 8218.
(42) Frisch, M. J.; Trucks, G. W.; Schlegel, H. B.; Scuseria, G. E.; Robb, M. A.; Cheeseman, J. R.; Zakrzewski, V. G.; Montgomery, J. A., Jr.; Stratmann, R. E.; Burant, J. C.; Dapprich, S.; Millam, J. M.; Daniels, A. D.; Kudin, K. N.; Strain, M. C.; Farkas, O.; Tomasi, J.; Barone, V.; Cossi, M.; Cammi, R.; Mennucci, B.; Pomelli, C.; Adamo, C.; Clifford, S.; Ochterski, J.; Petersson, G. A.; Ayala, P. Y.; Cui, Q.; Morokuma, K.; Malick, D. K.; Rabuck, A. D.; Raghavachari, K.; Foresman, J. B.; Cioslowski, J.; Ortiz, J. V.; Stefanov, B. B.; Liu, G.; Liashenko, A.; Piskorz, P.; Komaromi, I.; Gomperts, R.; Martin, R. L.; Fox, D. J.; Keith, T.; Al-Laham, M. A.; Peng, C. Y.; Nanayakkara, A.; Gonzalez, C.; Challacombe, M.; Gill, P. M. W.; Johnson, B. G.; Chen, W.; Wong, M. W.; Andres, J. L.; Head-Gordon, M.; Replogle, E. S.; Pople, J. A. *Gaussian 98*, revision A.6; Gaussian, Inc.: Pittsburgh, PA, 1998.
(43) For a critical and systematic evaluation of TD-DFT for the calculation of excitation energies in organic chromophores with the hybrid B3LYP functional, see Fabian, J.; Diaz, L. A.; Seifert, G.; Niehaus, T. *J. Mol. Struct.: THEOCHEM* **2002**, *594*, 41.
(44) (a) KappaCCD Operation Manual; Bruker Nonius BV: Delft, The Netherlands, 1997. (b) Sheldrick, G. M. *SHELXL97, Program for the Refinement of Crystal Structures*; University of Göttingen: Göttingen, Germany, 1997.

(CNRS) and the Ministère de l'Education Nationale, de la Recherche et de la Technologie.

Supporting Information Available: X-ray crystallographic data for structure determinations of **5**·HCl, **5**·2HCl·3$CHCl_3$, and **5**·HBF_4 (CIF). Cartesian coordinates of $\mathbf{5_H}$, $\mathbf{5_H}^+$, and $\mathbf{5_H}^{++}$ in their optimal geometries (DFT/BP86) (PDF). This material is available free of charge via the Internet at http://pubs.acs.org. The crystallographic material can also be obtained from the CCDC, the deposition numbers being CCDC 218698−218700.

JA035463U